Journal Pre-proof

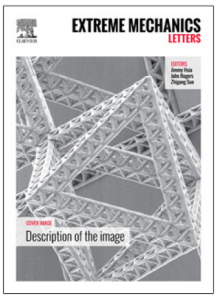

Data-driven continuum damage mechanics with built-in physics

Vahidullah Tac, Ellen Kuhl, Adrian Buganza Tepole

PII: S2352-4316(24)00100-7
DOI: https://doi.org/10.1016/j.eml.2024.102220
Reference: EML 102220

To appear in: *Extreme Mechanics Letters*

Received date : 5 April 2024
Revised date : 31 July 2024
Accepted date : 9 August 2024

Please cite this article as: V. Tac, E. Kuhl and A.B. Tepole, Data-driven continuum damage mechanics with built-in physics, *Extreme Mechanics Letters* (2024), doi: https://doi.org/10.1016/j.eml.2024.102220.

REVISED Manuscript (text UNmarked)

Graphical Abstract

Data-driven continuum damage mechanics with built-in physics

Vahidullah Tac, Ellen Kuhl, Adrian Buganza Tepole

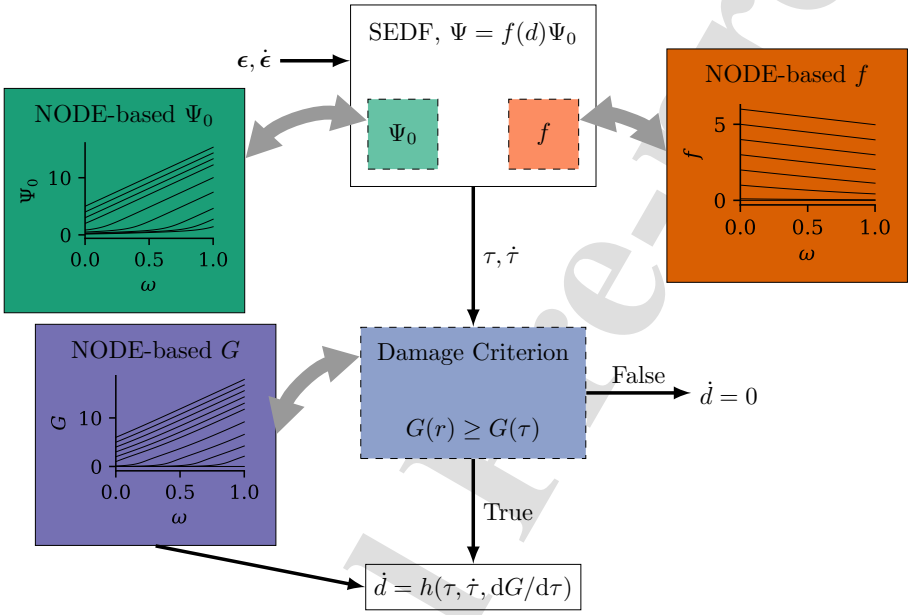

Highlights

Data-driven continuum damage mechanics with built-in physics

Vahidullah Tac, Ellen Kuhl, Adrian Buganza Tepole

- General, thermodynamically consistent data driven damage model
- Neural ODEs are used for monotonic yield functions
- The same deep learning architecture can learn various analytical models
- The deep learning framework can discover the correct damage functions from stress-deformation history data
- NODEs can capture experimental data of progressive tissue damage under cyclic loading

Data-driven continuum damage mechanics with built-in physics

Vahidullah Tac[a], Ellen Kuhl[b], Adrian Buganza Tepole[a,c]

[a] *School of Mechanical Engineering, Purdue University, West Lafayette, Indiana, USA*
[b] *Department of Mechanical Engineering, Stanford University, Stanford, California, USA*
[c] *Weldon School of Biomedical Engineering, Purdue University, West Lafayette, Indiana, USA*

Abstract

Soft materials such as rubbers and soft tissues often undergo large deformations and experience damage degradation that impairs their function. This energy dissipation mechanism can be described in a thermodynamically consistent framework known as continuum damage mechanics. Recently, data-driven methods have been developed to capture complex material behaviors with unmatched accuracy due to the high flexibility of deep learning architectures. Initial efforts focused on hyperelastic materials, and recent advances now offer the ability to satisfy physics constraints such as polyconvexity of the strain energy density function by default. However, modeling inelastic behavior with deep learning architectures and built-in physics has remained challenging. Here we show that neural ordinary differential equations (NODEs), which we used previously to model arbitrary hyperelastic materials with automatic polyconvexity, can be extended to model energy dissipation in a thermodynamically consistent way by introducing an inelastic potential: a monotonic yield function. We demonstrate the inherent flexibility of our network architecture in terms of different damage models proposed in the literature. Our results suggest that our NODEs re-discover the true damage function from synthetic stress-deformation history data. In addition, they can accurately characterize experimental skin and subcutaneous tissue data.

Keywords: physics-informed machine learning, neural ordinary differential equations, soft tissue mechanics, adipose tissue, skin biomechanics

1. Introduction

Physics-informed data driven constitutive modeling has allowed description of arbitrary materials with previously unmatched precision and within a unified framework [1, 2, 3, 4]. Machine learning constitutive modeling has gradually grown in complexity: Hyperelastic frameworks are fairly mature at this point [5]. Dissipative mechanisms have gained increasing attention recently, starting with deep learning frameworks to capture arbitrary linear elastoplastic yield functions [6, 7, 8, 9]. First efforts in the context of nonlinear inelasticity have been proposed, but mostly within the realm of model discovery, rather than deep learning [10, 11]. Currently, there is no deep learning framework for continuum damage mechanics at finite deformations and with built-in physics to simulate soft matter systems such as rubbers and tissues.

In the quest for data-driven models of soft materials, an important choice is between black-box approaches compared to model discovery out of a library of expert models [12, 13]. The route of model discovery has the advantage of yielding interpretable models, although it might compromise accuracy [1]. Deep learning architectures, on the other hand, take advantage of the universal approximation properties of fully connected neural networks to produce incredible flexible models at the cost of interpretability [1, 14, 15]. Some recent approaches aim at bridging these two classes of data-driven models [2, 16, 17, 18]. Model discovery also has the benefit of guaranteeing physics constraints by default. For black-box approaches, physics can be added in the loss function or directly into the architecture. The latter is, of course, preferable and has become the method of choice [19].

In our previous work, we introduced a deep learning method with built-in polyconvexity for hyperelastic materials based on neural ordinary differential equations (NODEs) [20]. The reasoning behind our approach relies on two observations: that ODEs can be used to construct monotonic functions, and that stress data depend on energy derivatives rather than the energy function itself. Hence, we used NODEs to build monotonic strain energy derivative functions that represent an underlying polyconvex strain energy [20]. More recently we extended our framework to finite deformation nonequilibrium viscoelasticity by introducing a convex dissipation potential, also modeled with NODEs [14]. The method is flexible and able to capture a wide range of soft materials, biological and non biological, such as brain, rubber, myocardium, and fibrin gels.

Biological tissues and soft materials like rubber display other forms of dissipation in addition to viscoelastic behavior [21]. In rubbers, energy dissipation due to damage is known as the Mullins effect [22, 23]. When first loaded from a stress-free, virgin state, rubber materials display a characteristic stress-stretch response. When unloaded and loaded again to the same maximum deformation, the curve of the second loading will be underneath the first one. More importantly, this is only seen in between the first and the second cycles. If unloaded and loaded a third time to the same maximum deformation as before, the third and second curves will overlap. In other words, the damage is a function of the previously experienced maximum deformation [23]. In the context of linear elastic materials with incremental rate equations for damage accumulation, stiffness loss is understood as creation of voids or micro-cracks, which reduce the effective load carrying area [24, 25]. In the context of large deformations in nonlinear materials, the thermodynamically consistent framework to characterize these effects is known as continuum damage mechanics [26, 27]. By defining the free energy as a function of the deformation and the damage state of the material, appropriate thermodynamic conjugate variables arise, with clear conditions for the satisfaction of the second law of thermodynamics. In the case of damage, the conjugate variable to the damage variable is proportional to the undamaged strain energy [26], and a monotonic yield function, similar to plasticity, guarantees positive energy dissipation [28].

In the present work, we present a fully data-driven model of continuum damage mechanics with built-in physics: polyconvexity of the strain energy function and positive, irreversible dissipation in response to damage accumulation. The method extends our previous work on NODE models of hyperelastic materials by incorporating additional NODEs to construct monotonic yield functions. We demonstrate the applicability of the same architecture to capture a variety of closed-form damage models from the literature. In addition, we apply our methods to experimental data from skin and adipose tissue.

2. Materials and Methods

We follow the thermodynamic consistent continuum damage mechanics approach [26]. We begin with a free energy potential that consists of n

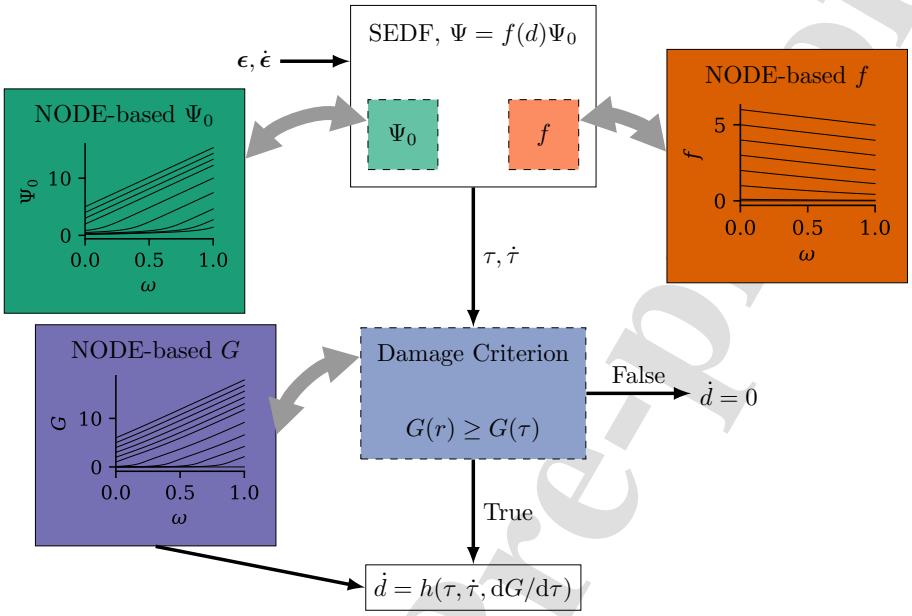

Figure 1: Overview of the proposed data-driven inelastic damage model with built-in physics.

additive parts $\Psi_j, j \in [1, n_{\text{fibers}} + 3]$ as

$$\Psi(\mathbf{C}, \mathbf{d}) = f_1(d_1)\Psi_1^o(I_1) + f_2(d_2)\Psi_2^o(I_2) + f_3(d_3)\Psi_3^o(J) + \sum_{i=1}^{n_{\text{fibers}}} f_{i+3}(d_{i+3})\Psi_{i+3}^o(I_{4,i}) \tag{1}$$

where $\mathbf{d} = \{d_1, \cdots, d_n\}$ are the damage variables, f_j is the function that characterizes the change in the energy function with a change in d_j, I_1 and I_2 are the first two principal invariants of the right Cauchy Green deformation tensor $\mathbf{C} = \mathbf{F}^T\mathbf{F}$ with determinant $J = \sqrt{\det \mathbf{C}}$, and $I_{4,i}$ are anisotropic invariants defined in terms of fiber direction vectors $\mathbf{v}_i$, as $I_{4,i} = \mathbf{v}_i\mathbf{C}\mathbf{v}_i$. This additive decomposition includes the single scalar damage model [26], but extends it to a more general setting. For instance, fiber damage models for anisotropic materials such as collagen reinforced models typically incorporate additional damage variables [29, 30]. Conceptually, different damage mechanisms could lead to different energy losses associated with different deformation modes or different constituents.

The Clausius-Duhem inequality for isothermal processes reads

$$\begin{aligned}\mathcal{D} &= \frac{1}{2}\mathbf{S} : \dot{\mathbf{C}} - \dot{\Psi} \geq 0 \\ &= \frac{1}{2}\mathbf{S} : \dot{\mathbf{C}} - \left(\frac{\mathrm{d}\Psi_1^o}{\mathrm{d}I_1}\frac{\mathrm{d}I_1}{\mathrm{d}\mathbf{C}} + \frac{\mathrm{d}\Psi_2^o}{\mathrm{d}I_1}\frac{\mathrm{d}I_2}{\mathrm{d}\mathbf{C}} + \cdots\right) : \dot{\mathbf{C}} - \Psi_1^o\frac{\mathrm{d}f_1}{\mathrm{d}d_1} - \Psi_2^o\frac{\mathrm{d}f_2}{\mathrm{d}d_2} - \cdots \geq 0 \\ &= \frac{1}{2}\left(\mathbf{S} - 2\frac{\mathrm{d}\Psi_1^o}{\mathrm{d}I_1}\frac{\mathrm{d}I_1}{\mathrm{d}\mathbf{C}} - 2\frac{\mathrm{d}\Psi_2^o}{\mathrm{d}I_1}\frac{\mathrm{d}I_2}{\mathrm{d}\mathbf{C}} - \cdots\right) : \dot{\mathbf{C}} - \Psi_1^o\frac{\mathrm{d}f_1}{\mathrm{d}d_1} - \Psi_2^o\frac{\mathrm{d}f_2}{\mathrm{d}d_2} - \cdots \geq 0\end{aligned} \tag{2}$$

where

$$-Y_i = -\frac{\partial\Psi}{\partial d_i} = -\Psi_i^o\frac{\mathrm{d}f_i}{\mathrm{d}d_i}$$

is the conjugate thermodynamic force to the damage variable d_i. Here we enforce the non-negativity of the dissipation independently for each term in (2), i.e.,

$$-Y_i = -\Psi_i^o\frac{\mathrm{d}f_i}{\mathrm{d}d_i} \geq 0, \quad i \in [1, n]\,.$$

Since the energy Ψ_i^o is always positive, f_i must be a *non-increasing* function of d_i. The condition of positivity of Ψ (Eq. (1)) also implies that $f_i(d_i) > 0$. Furthermore, it is convenient to require that $f_i(0) = 1$, such that Ψ_i^o defines the virgin, undamaged state of the material. In summary, $f_i(d_i)$ must satisfy the following conditions,

$$f_i : R^+ \to [0, 1], \quad f_i(0) = 1, \quad f_i \text{ non-increasing} \tag{3}$$

We previously showed that Neural ODEs (NODEs) can be used to construct monotonic functions and they can easily be modified to map 0 to 0. Following this, we propose two alternatives for f_i. In the more general case we could implement a data-driven form for f_i,

$$f_i(d_i) = e^{-\mathcal{N}_i(d_i)}$$

where $\mathcal{N}_i$ would be a NODE. It is trivial to see that the requirements in (3) are satisfied with this form. In practice, the additional degrees of freedom in this decay function are not necessary provided there is enough flexibility in the yield function. The more traditional approach, and the one we follow in the examples below, is to simply scale the energy linearly with respect to the damage,

$$f_i(d_i) = 1 - d_i\,.$$

2.1. Damage evolution

We hypothesize that damage in the material only accumulates when the level of deformation reaches a threshold or yield criterion [26], which in turn grows with loading. We denote the corresponding thermodynamic conjugate, $-Y_i \equiv \tau_i$, and determine the change of each damage variable, d_i. To this end, we introduce damage criteria g_i of the form

$$g_i(\tau_i(t), r_i(t)) = G_i(\tau_i) - G_i(r_i) \leq 0$$

where $G_i(\cdot)$ is a monotonically increasing function and $r_i(t)$ is the current value of the threshold for τ_i. We define the evolution of the damage variable d_i as

$$\begin{aligned} \dot{d}_i(t) &= \dot{\mu}_i \frac{\partial g_i(\tau_i, r_i)}{\partial \tau_i} = \dot{\mu}_i \frac{\mathrm{d}G_i(\tau_i)}{\mathrm{d}\tau_i} \\ \dot{r}_i(t) &= \dot{\mu}_i(t) \end{aligned} \tag{4}$$

where $\dot{\mu}_i$ is a damage consistency parameter that has to satisfy the Kuhn-Tucker conditions of the irreversible damage process [31],

$$\dot{\mu}_i \geq 0, \quad g_i(\tau_i, r_i) \leq 0, \quad \dot{\mu}_i g_i(\tau_i, r_i) = 0\,. \tag{5}$$

If $g_i(\tau_i, r_i) < 0$, no damage takes place and $\dot{d}_i = \dot{r}_i = \dot{\mu}_i = 0$ by $(5)_3$. If, on the other hand, damage accumulates, $\dot{\mu} > 0$, then $g_i(\tau_i, r_i) = \dot{g}_i(\tau_i, r_i) = 0$,

$$g_i(\tau_i, r_i) = 0 = G_i(\tau_i) - G_i(r_i) \implies r_i = \tau_i$$

$$\begin{aligned} \dot{g}_i(\tau_i, r_i) = 0 = & \frac{\mathrm{d}G_i(\tau_i)}{\mathrm{d}t} - \frac{\mathrm{d}G_i(r_i)}{\mathrm{d}t} \\ \implies & \left.\frac{\mathrm{d}G_i(\tau_i)}{\mathrm{d}\tau_i}\right|_{\tau_i = r_i} \dot{\tau}_i = \left.\frac{\mathrm{d}G_i(r_i)}{\mathrm{d}r_i}\right|_{\tau_i = r_i} \dot{r}_i \\ \implies & \dot{r}_i = \dot{\tau}_i \end{aligned}$$

and by $(4)_2$, $\dot{\mu} = \dot{r}$. By combining this consideration with the evolution rule of $(4)_1$, we obtain the damage evolution law,

$$\dot{d}_i = \dot{\tau}_i \frac{\mathrm{d}G_i(\tau_i)}{\mathrm{d}\tau_i}\,. \tag{6}$$

Note that when $f_i(d_i) = 1 - d_i$, $\dot{\tau}_i$ does not depend on d_i, and (6) is an explicit expression for $\dot{d}_i$. However, for general f_i,

$$\dot{\tau}_i = \frac{\mathrm{d}}{\mathrm{d}t}\left(-\Psi_i^o \frac{\mathrm{d}f_i}{\mathrm{d}d_i}\right) = -\dot{\Psi}_i^o \frac{\mathrm{d}f_i}{\mathrm{d}d_i} - \Psi_i^o \frac{\mathrm{d}^2 f_i}{\mathrm{d}d_i^2}\dot{d}_i$$

and

$$\dot{d}_i = -\left(\dot{\Psi}_i^o \frac{\mathrm{d}f_i}{\mathrm{d}d_i}\frac{\mathrm{d}G_i}{\mathrm{d}\tau_i}\right)\left(1 + \Psi_i^o \frac{\mathrm{d}^2 f_i}{\mathrm{d}d_i^2}\frac{\mathrm{d}G_i}{\mathrm{d}\tau_i}\right)^{-1}.$$

Since G_i has to satisfy the condition of monotonicity, we propose modeling G with Neural ODEs as

$$G_i(\tau_i) = \mathcal{N}_i(\tau_i)\,. \tag{7}$$

2.2. Closed-form damage models

Most existing damage models propose an simple analytical function to specify the evolution of damage. This can either be incremental evolution equations [26, 32], or d can be specified explicitly as a function of conjugate variable without a rate equation [33, 34]. Here we define d implicitly in terms of Eq. (6). Note that under monotonic loading, in the absence of unloading, r_i and τ_i are equivalent and we can write Eq. (6) in terms of r_i.

Different types of damage evolution have been proposed in the literature [35, 36, 28]. For example, damage can evolve according to [35],

$$d = \exp(-\exp(\eta(r^d - r)))\,, \tag{8}$$

where η is a material parameter and r^d is a threshold beyond which damage occurs. Another exponential equation [36] characterizes damage evolution as,

$$d = 1 - \exp(-\eta < r - r^d >)\,, \tag{9}$$

where η is again a material parameter and $< \bullet >= \max\{0, \bullet\}$ denotes the Macaulay bracket function. An alternative evolution equation [28] takes the following form,

$$d = d_\infty(\,1 - \exp\left(r/\beta\right)\,)\,. \tag{10}$$

These are only three examples that we will use to illustrate the versatility of our method to capture damage models from the literature [28].

2.3. Model calibration and verification

2.3.1. Training against closed form model directly

To show that the NODE framework is able to capture closed form models, the first calibration is to fit a NODE directly to the damage functions Eqs. (8)-(10). Input data is thus sampling of r values, and labeled output data are $\dot{d}(r)$ for a specific model from Eqs. (8)-(10). Because an analytical function is available, $N = 50$ equally-spaced r values are selected as inputs. The loss is directly the mean squared error between predicted and the ground truth analytical model $\sum_{j=1}^{N}(\dot{d}_j^{pred} - \dot{d}_j^{gt})/N$, where the predicted damage comes from (6) using Eq. (7). The models are trained for 100000 epochs with the built in JAX ADAMS optimizer with initial learning rate 5×10^{-4} [37]. No batching is used. The architecture used for the NODE is $1 \times 5 \times 5 \times 5 \times 1$. The NODE is integrated in pseudo-time $s \in [0, 1]$ with the 4^{th} order Runge-Kutta integrator. For validation, to test if fitting directly to the damage functions Eqs. (8)-(10) is able to reproduce accurate stress-strain behavior, we then use the trained model Eq. (7) in cyclic loading to progressively larger stretches and evaluate the damage evolution and stress-stretch response.

2.3.2. Training on stress history data generated with analytical models

As a second validation exercise, we propose the more challenging task of discovering the damage model from observed stress-strain history data. The same analytical damage models Eqs. (8)-(10) are used to generate the stress history data from 3 cycles of loading to progressively larger stretch. A total of $N = 300$ stress-stretch values are saved for equally-spaced loading steps in the time interval $t \in [0, 6]$s, 100 points and 2s for each cycle. For the loss in this case, the NODE model is used via Eq. (7) to evolve the damage over time as a function of the imposed loading. For the strain energy density function, an NODE model is used. The loss is the mean squared error between predicted and observed stress histories $\sum_{j=1}^{N}(\sigma_j^{pred} - \sigma_j^{gt})^2/N$. The entire stress history is used in every epoch. The loss is minimized over 100000 epochs, with the same optimizer parameters as before. The NODE also has the same architecture as in the previous subsection. To validate that the discovered model is indeed the one used to generate the stress history data, we compare the learned Eq.(7) against $d(r)$ from Eqs. (8)-(10).

2.3.3. Experimental data

We have previously characterized damage of subcutaneous and dermis tissue [38, 39]. For these experiments, the tissues were loaded uniaxially at

a given stretch λ_s^{max} where s denotes the stages of loading. Five stages were performed, $\lambda_s \in [1.3, 1.35, 1.4, 1.45, 1.5]$, for the dermis, with five repetitions at each stage. The reason for the multiple cycles at a given maximum stretch before proceeding to the next λ_s is that tissues display pre-conditioning that we attribute to the dissipation associated with viscoelastic relaxation and damage [40]. Since we are only interested in the damage response in this manuscript, we only use the unloading down-stroke at the end of each loading stages and ignore the remaining cyclic data during training. For the subcutaneous tissue, the maximum stretches at each stage of loading are $\lambda_s \in [1.4, 1.5, 1.6, 1.7, 1.5]$. Again, only the down-stroke (unloading) stress-stretch data is available for model training. Because there is no damage accumulation during unloading, the fitting procedure is done in two stages. First, a data-driven strain energy as well as independent $d^{(s)}$ values are fitted to the stress data. The notation $d^{(s)}$ distinguishes the value of the damage at the stages of loading, $\lambda_s \in [1.3, 1.35, 1.4, 1.45, 1.5]$ or $\lambda_s \in [1.4, 1.5, 1.6, 1.7, 1.5]$, from the notation d_i used previously for different damage mechanisms. After fitting Ψ_i^o (or rather its derivative) and the scalars $d^{(s)}$, we proceed to construct a data-driven damage function able to capture the $d^{(s)}$. Because of the exponential nature of collagenous tissue loading, the strain energy function is modeled with a scaling $\partial\Psi_0/\partial I_i = \exp(\mathcal{N}_i(I_i))$ where $\mathcal{N}_i$ denotes a NODE. To train the $G(\circ)$ functions, we use $G_i(\tau_i) = \tanh(a\mathcal{N}(\tau_i)$, with $a = \exp(\hat{a})$ and $\hat{a}$ a trainable parameter. There are $5 \times 50 = 250$ data points for dermis and $4 \times 126 = 504$ for subcutaneous tissue, all of which are used in each epoch. The model is trained first for 100000 epochs with the JAX ADAM optimizer learning rate of 5×10^{-4} to obtain Ψ^o, then for 15000000 epochs to learn G. The NODE architecture for the Ψ^o is $1 \times 3 \times 3 \times 3 \times 1$ while for G it is $1 \times 5 \times 5 \times 5 \times 1$. The same architecture and training procedure is used for the subcutaneous tissue. The overall training time is less than 1 hour on an Apple M1 Pro CPU.

3. Results

3.1. Learning closed-form damage evolution functions

As outlined in the Methods section, we first train $G(r)$, the yield function, directly based on the analytical models $d(r)$ from Eqs. (8)-(10). The results are depicted in Fig. 2. The NODE model, unsurprisingly, is able to capture $d(r)$ perfectly. The more challenging task is to then predict stress histories

with the trained NODE and compare against ones generated with the analytical equations. This is shown in Fig. 2, right. We simulate uniaxial tension for 3 cycles of increasing maximum deformation. Damage accumulates only during the loading parts of the cycle, with d remaining at a constant value during unloading. In the second cycle, once the maximum deformation goes past the previously experienced maximum deformation, damage accumulates again. For the stress history, this implies that even in the first cycle, the unloading path falls beneath the first loading path. Then, during the second cycle, the loading path follows the unloading path of the first cycle up to the previously observed maximum stress. At at that point damage starts accumulating again. Unloading once more falls beneath the previous loading curve and so on. All three models Eqs. (8)-(10) show a similar evolution of damage during the loading history $d(t)$, yet, the stress history shows some qualitative differences in Fig. 2, right. Namely, while the three models dissipate energy such that the material losses stiffness, the effect is more pronounced for Eq. (8), less so for Eq. (9), and even more subtle for Eq. (10). For Eq. (8), d approaches 1 rapidly, leading to appreciable softening of the material, observed in failure of collagenous soft tissues [41].

3.2. Discovering the damage evolution function from stress-deformation histories

The second, more challenging task, is discovering the damage model from the stress-stretch history data. These results are shown in Fig. 3. The same data as in Fig. 2, right, is used: stress history from 3 cycles with increasing maximum stretch using Eqs. (8)-(10). Trained directly on these data, the NODE damage model learns a yield function $G(r)$ such that the stress history is matched accurately, see Fig. 3, left. More importantly, when plotting the discovered $G(r)$ by the NODE agains the ground truth Eqs. (8)-(10), it can be observed in Fig. 3, right, that the NODE model is able to discover the underlying damage model even though Eqs. (8)-(10) were not directly used in training.

3.3. Application to experimental data

Moving past analytical examples and synthetically generated stress history data, here we train the NODE strain energy and yield models against experimental data of dermis and subcutaneous tissue from [38, 39]. Note that only unloading data is available for training. During unloading, damage does not accumulate. As described in the Methods section, we trained in

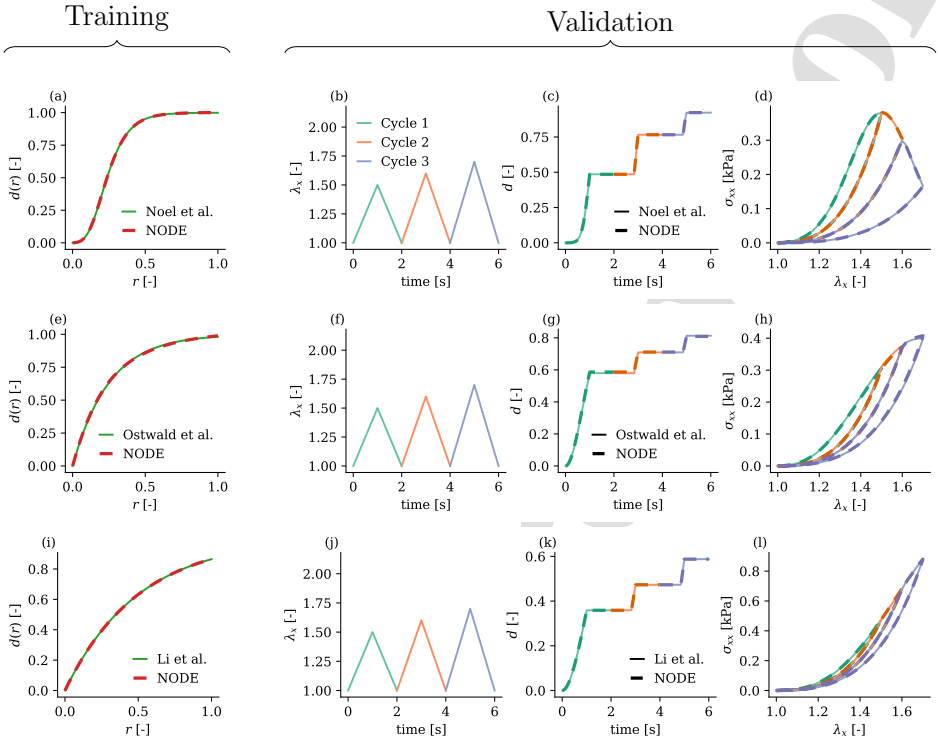

Figure 2: Training against closed-form damage functions. We train $G(r)$ with a NODE model, to match the analytical functions $d(r)$ from Eqs. Eqs. (8)-(10). The NODE matches the analytical model. For validation, we simulate uniaxial cyclic loading to increasing maximum stretch using either the analytical functions Eqs. (8)-(10) or the trained NODE model. Predictions of stress history also match exactly the ground truth, capturing the energy dissipation due to damage which leads to loss of stiffness and even softening.

two steps. For the dermis, in the first step we trained the strain energy Ψ^o (or rather its derivative) and five scalar parameters $d^{(s)}$, one for each of the unloading curves from the loading depicted in Fig. 4a. The damage evolution function $G(r)$ was trained in a second step based on the $d^{(s)}$ values. The comparison between the data-driven model and experimental stress data is shown in Fig. 4b, while the learned damage evolution function is shown in Fig. 4c. A similar training strategy was used for the subcutaneous tissue data. In this case, only four unloading curves were available, from a loading path illustrated in Fig. 5a. The predicted stress history data during the

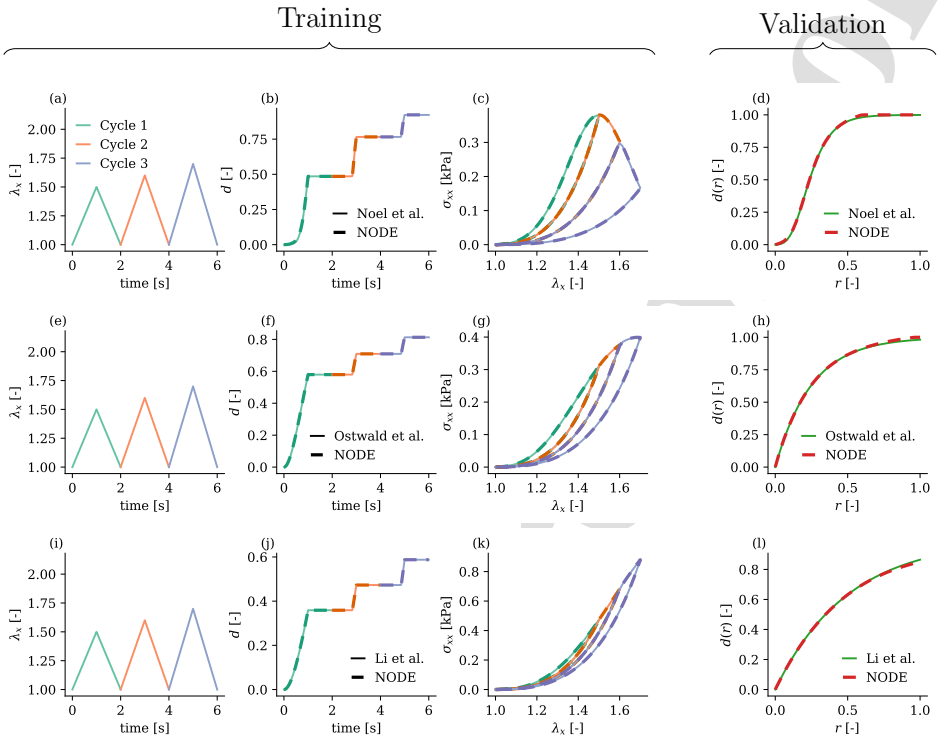

Figure 3: Training with stress-stretch history data. Using analytical models Eqs. (8)-(10), stress data was generated by simulating three cycles of uniaxial extension to increasing maximum deformation. The NODE model $G(r)$ was trained by simulating the same cyclic uniaxial loading protocol with the NODE $G(r)$ and comparing the predicted stress history against the ground truth. By minimizing this loss during training (left), the NODE discovers the ground truth Eqs. (8)-(10), right.

entire loading path is shown in Fig. 5b, together with the experimental data from the unloading portions of the test. The data-driven model is able to accurately match the experiments in Fig. 5b. The discovered damage function is shown in Fig. 5c.

4. Discussion

We propose a data-driven method to model energy dissipation due to damage by introducing a damage variable that monotonically decreases the strain energy capacity of the material. The evolution of the damage is driven

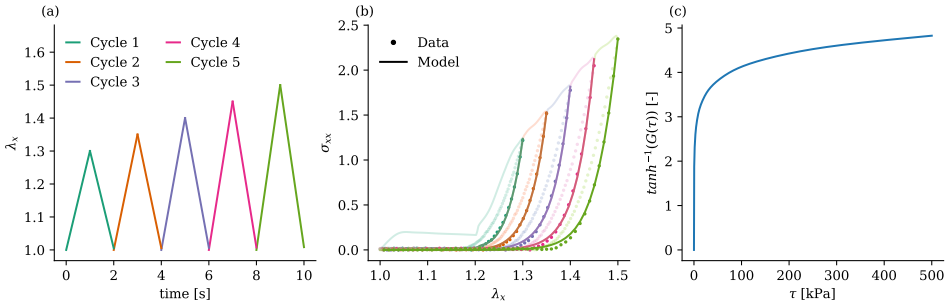

Figure 4: NODE model accurately captures the damage response of dermis tissue from cyclic loading data to increasing maximum deformations. The transparent plots correspond to the predicted paths for loading. No data was available for the loading portion of the tests, only the unloading was recorded and used for training.

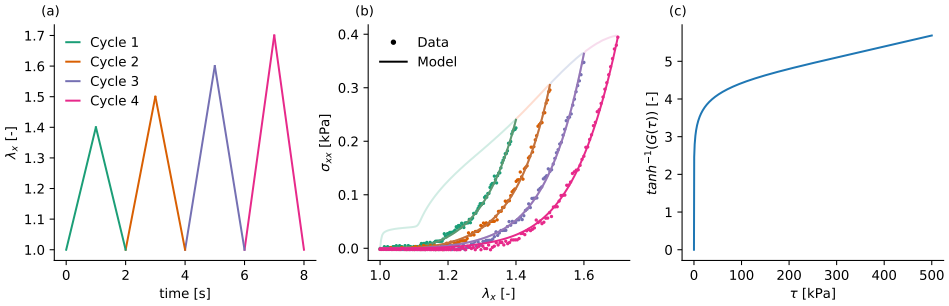

Figure 5: NODE model accurately captures the damage response of subcutaneous tissue from cyclic loading data to increasing maximum deformations. The transparent plots correspond to the predicted paths for loading. No data was available for the loading portion of the tests, only the unloading was recorded and used for training.

by its thermodynamic conjugate variable through a data-driven yield potential based on NODEs which is monotonic by design. Paired with our previous data-driven modeling framework for automatically polyconvex strain energies, the method is fully data-driven and extremely flexible, which allows it to capture multiple analytical models in the literature as well as experimental data of soft tissue damage.

Not all damage models for soft nonlinear materials are based on energy and dissipation potentials. The pseudoelastic modeling approach by Ogden is extremely popular [23], as well as its extension to hydrogels [42] and

anisotropic materials [43, 44]. Significant effort has been done for multi-scale and micromechanics approaches to describe damage [45, 46, 47]. The work here more closely aligns with phenomenological models of soft tissue damage, such as the ones we used in the synthetic data examples [35, 36, 28], or other similar efforts in the literature [48, 49]. Connection to micromechanics approaches is an interesting area of future investigation. For instance, we could envision an explicit description of the microstructure geometry [38], but with a data-driven framework for the damage evolution of individual fibers. Here, the thermodynamic conjugate variable is the undamaged strain energy because the response of the material is modeled as a scaling of this virgin strain energy by a monotonically decreasing damage function [26]. Alternatively, internal variables that do not scale the energy but rather modify the functional form are also possible [50, 51].

Here we work with NODEs because they span a suitable space of monotonic functions to capture both the strain energy derivatives as well as the damage evolution criteria. However, NODEs are not the only way of imposing the desired physics. For the polyconvexity of the strain energy with the black-box approaches–as opposed to the model discovery strategy [12]– the most popular alternative to NODEs are input convex neural networks [1, 19]. For the yield function, convexity is not needed, monotonicity is sufficient. Monotonic neural networks are an alternative to NODEs [52].

One limitation of the present work is the focus on the damage model itself without addressing its numerical implementation into simulations. Additional considerations might be important when implementing the data-driven damage model into numerical solvers because of potential damage localization [53]. To avoid damage localization problems, gradient based approaches are popular [54, 55]. Thus, future work will look into computational implementation with likely extension to gradient-based damage models [56]. Additionally, a more thorough benchmarking exercise against a wider set of damage modeling approaches and with a broader dataset is needed. In this manuscript we showed that the NODE model is able to capture popular phenomenological damage models and it is able to capture skin and subcutaneous tissue data. Yet, a more thorough comparison should include microstructure-based approaches [29, 30], and other soft materials and tissues [57, 58].

Taken together, this work contributes to the evolving field of data-driven constitutive modeling by introducing a flexible and generic framework for continuum damage mechanics based on NODEs. The method does not make

any assumption regarding the underlying strain energy or damage evolution functions; yet, by design, it enforces the physical requirement of positive energy dissipation during damage in addition to the polyconvexity of the strain energy. Damage mechanisms are particularly important for soft materials such as tissues, hydrogels, and bioprinted materials, especially for applications that requiring repetitive loading, for example in heart valve replacements [59]. We anticipate that our unifying data-driven framework will enable widespread accurate prediction of soft material damage in realistic applications without the limitations and burdens of expert-constructed models.

5. Acknowledgements

ABT acknowledges support from National Institute of Arthritis and Musculoskeletal and Skin Diseases, National Institute of Health, United States under award R01AR074525.

6. Declarations

The authors have no conflicts of interest to declare.

7. Supplementary material

All data, model parameters and code associated with this study are available in a public Github repository at `https://github.com/tajtac/node_damage`.

References

[1] V. Taç, K. Linka, F. Sahli-Costabal, E. Kuhl, A. B. Tepole, Benchmarking physics-informed frameworks for data-driven hyperelasticity, Computational Mechanics (Jun. 2023). doi:10.1007/s00466-023-02355-2.

[2] K. Linka, E. Kuhl, A new family of constitutive artificial neural networks towards automated model discovery, Computer Methods in Applied Mechanics and Engineering 403 (2023) 115731.

[3] J. N. Fuhg, N. Bouklas, On physics-informed data-driven isotropic and anisotropic constitutive models through probabilistic machine learning and space-filling sampling, Computer Methods in Applied Mechanics and Engineering 394 (2022) 114915.

[4] N. N. Vlassis, R. Ma, W. Sun, Geometric deep learning for computational mechanics part i: anisotropic hyperelasticity, Computer Methods in Applied Mechanics and Engineering 371 (2020) 113299. doi:https://doi.org/10.1016/j.cma.2020.113299.

[5] H. Jin, E. Zhang, H. D. Espinosa, Recent advances and applications of machine learning in experimental solid mechanics: A review, Applied Mechanics Reviews 75 (6) (2023) 061001.

[6] J. N. Fuhg, C. M. Hamel, K. Johnson, R. Jones, N. Bouklas, Modular machine learning-based elastoplasticity: Generalization in the context of limited data (Oct. 2022). arXiv:2210.08343.

[7] N. N. Vlassis, W. Sun, Sobolev training of thermodynamic-informed neural networks for interpretable elasto-plasticity models with level set hardening, Computer Methods in Applied Mechanics and Engineering 377 (2021).

[8] M. Rosenkranz, K. A. Kalina, J. Brummund, M. Kästner, A comparative study on different neural network architectures to model inelasticity, International Journal for Numerical Methods in Engineering 124 (21) (2023) 4802–4840.

[9] W. G. Dettmer, E. J. Muttio, R. Alhayki, D. Perić, A framework for neural network based constitutive modelling of inelastic materials, Computer Methods in Applied Mechanics and Engineering 420 (2024) 116672.

[10] H. Holthusen, L. Lamm, T. Brepols, S. Reese, E. Kuhl, Theory and implementation of inelastic constitutive artificial neural networks, arXiv preprint arXiv:2311.06380 (2023).

[11] P. Thakolkaran, A. Joshi, Y. Zheng, M. Flaschel, L. De Lorenzis, S. Kumar, Nn-euclid: Deep-learning hyperelasticity without stress data, Journal of the Mechanics and Physics of Solids 169 (2022) 105076.

[12] M. Flaschel, S. Kumar, L. De Lorenzis, Unsupervised discovery of interpretable hyperelastic constitutive laws, Computer Methods in Applied Mechanics and Engineering 381 (2021) 113852. doi:10.1016/j.cma.2021.113852.

[13] G. A. Holzapfel, K. Linka, S. Sherifova, C. J. Cyron, Predictive constitutive modelling of arteries by deep learning, Journal of the Royal Society Interface 18 (182) (2021) 20210411.

[14] V. Taç, M. K. Rausch, F. S. Costabal, B. Tepole, Data-driven anisotropic finite viscoelasticity using neural ordinary differential equations, Computer Methods in Applied Mechanics and Engineering 411 (2023).

[15] P. Chen, J. Guilleminot, Polyconvex neural networks for hyperelastic constitutive models: A rectification approach, Mechanics Research Communications 125 (2022) 103993.

[16] V. Tac, V. D. Sree, M. K. Rausch, A. B. Tepole, Data-driven modeling of the mechanical behavior of anisotropic soft biological tissue, Engineering with Computers 38 (5) (2022) 4167–4182.

[17] B. Bahmani, H. S. Suh, W. Sun, Discovering interpretable elastoplasticity models via the neural polynomial method enabled symbolic regressions, Computer Methods in Applied Mechanics and Engineering 422 (2024) 116827.

[18] G. Bomarito, T. Townsend, K. Stewart, K. Esham, J. Emery, J. Hochhalter, Development of interpretable, data-driven plasticity models with symbolic regression, Computers & Structures 252 (2021) 106557.

[19] F. As' ad, P. Avery, C. Farhat, A mechanics-informed artificial neural network approach in data-driven constitutive modeling, International Journal for Numerical Methods in Engineering 123 (12) (2022) 2738–2759.

[20] V. Tac, F. Sahli Costabal, A. B. Tepole, Data-driven tissue mechanics with polyconvex neural ordinary differential equations, Computer Methods in Applied Mechanics and Engineering 398 (2022) 115248. doi:https://doi.org/10.1016/j.cma.2022.115248.

[21] X. Zhao, Multi-scale multi-mechanism design of tough hydrogels: building dissipation into stretchy networks, Soft matter 10 (5) (2014) 672–687.

[22] L. Mullins, Effect of stretching on the properties of rubber, Rubber chemistry and technology 21 (2) (1948) 281–300.

[23] R. W. Ogden, D. G. Roxburgh, A pseudo–elastic model for the mullins effect in filled rubber, Proceedings of the Royal Society of London. Series A: Mathematical, Physical and Engineering Sciences 455 (1988) (1999) 2861–2877.

[24] C. Chow, T. Lu, On evolution laws of anisotropic damage, Engineering Fracture Mechanics 34 (3) (1989) 679–701.

[25] I. Carol, E. Rizzi, K. Willam, On the formulation of anisotropic elastic degradation. i. theory based on a pseudo-logarithmic damage tensor rate, International Journal of Solids and Structures 38 (4) (2001) 491–518.

[26] J. C. Simo, J. Ju, Strain-and stress-based continuum damage models—i. formulation, International journal of solids and structures 23 (7) (1987) 821–840.

[27] M. Sumio, Continuum damage mechanics: A continuum mechanics approach to the analysis of damage and fracture (2012).

[28] W. Li, Damage models for soft tissues: a survey, Journal of Medical and Biological Engineering 36 (2016) 285–307.

[29] J. D. Toaquiza Tubon, O. Moreno-Flores, V. D. Sree, A. B. Tepole, Anisotropic damage model for collagenous tissues and its application to model fracture and needle insertion mechanics, Biomechanics and Modeling in Mechanobiology 21 (6) (2022) 1–16.

[30] M. K. Rausch, J. D. Humphrey, A microstructurally inspired damage model for early venous thrombus, Journal of the mechanical behavior of biomedical materials 55 (2016) 12–20.

[31] I. Einav, G. Houlsby, G. Nguyen, Coupled damage and plasticity models derived from energy and dissipation potentials, International Journal of Solids and Structures 44 (7-8) (2007) 2487–2508.

[32] V. Alastrué, J. Rodríguez, B. Calvo, M. Doblaré, Structural damage models for fibrous biological soft tissues, International Journal of solids and Structures 44 (18-19) (2007) 5894–5911.

[33] D. Balzani, J. Schröder, D. Gross, Simulation of discontinuous damage incorporating residual stresses in circumferentially overstretched atherosclerotic arteries, Acta biomaterialia 2 (6) (2006) 609–618.

[34] N. Famaey, J. Vander Sloten, E. Kuhl, A three-constituent damage model for arterial clamping in computer-assisted surgery, Biomechanics and modeling in mechanobiology 12 (2013) 123–136.

[35] L. Noël, E. Kuhl, Modeling neurodegeneration in chronic traumatic encephalopathy using gradient damage models, Computational Mechanics 64 (5) (2019) 1375–1387.

[36] R. Ostwald, E. Kuhl, A. Menzel, On the implementation of finite deformation gradient-enhanced damage models, Computational Mechanics 64 (2019) 847–877.

[37] J. Bradbury, R. Frostig, P. Hawkins, M. J. Johnson, C. Leary, D. Maclaurin, G. Necula, A. Paszke, J. VanderPlas, S. Wanderman-Milne, Q. Zhang, JAX: composable transformations of Python+NumPy programs (2018).
URL `http://github.com/google/jax`

[38] V. D. Sree, J. D. Toaquiza-Tubon, J. Payne, L. Solorio, A. B. Tepole, Damage and fracture mechanics of porcine subcutaneous tissue under tensile loading, Annals of Biomedical Engineering 51 (9) (2023) 2056–2069.

[39] J. T. Tubon, V. D. Sree, J. Payne, L. Solorio, A. B. Tepole, Mechanical damage in porcine dermis: Micro-mechanical model and experimental characterization, Journal of the Mechanical Behavior of Biomedical Materials 147 (2023) 106143.

[40] O. Lokshin, Y. Lanir, Viscoelasticity and preconditioning of rat skin under uniaxial stretch: microstructural constitutive characterization (2009).

[41] S. Bose, S. Li, E. Mele, V. V. Silberschmidt, Fracture behaviour and toughening mechanisms of dry and wet collagen, Acta Biomaterialia 142 (2022) 174–184.

[42] T. Zhang, S. Lin, H. Yuk, X. Zhao, Predicting fracture energies and crack-tip fields of soft tough materials, Extreme Mechanics Letters 4 (2015) 1–8.

[43] S. Göktepe, C. Miehe, A micro–macro approach to rubber-like materials. part iii: The micro-sphere model of anisotropic mullins-type damage, Journal of the Mechanics and Physics of Solids 53 (10) (2005) 2259–2283.

[44] T.-T. Mai, Y. Morishita, K. Urayama, Induced anisotropy by mullins effect in filled elastomers subjected to stretching with various geometries, Polymer 126 (2017) 29–39.

[45] R. Y. Dhume, E. D. Shih, V. H. Barocas, Multiscale model of fatigue of collagen gels, Biomechanics and modeling in mechanobiology 18 (1) (2019) 175–187.

[46] F. Burla, S. Dussi, C. Martinez-Torres, J. Tauber, J. van der Gucht, G. H. Koenderink, Connectivity and plasticity determine collagen network fracture, Proceedings of the National Academy of Sciences 117 (15) (2020) 8326–8334.

[47] N. Witt, A. Woessner, J. Herrmann, K. Quinn, E. Sander, Mechanical models of collagen networks for understanding changes in the failure properties of aging skin, Journal of biomechanical engineering (2024) 1–28.

[48] P. Sáez, V. Alastrué, E. Pena, M. Doblaré, M. Martínez, Anisotropic microsphere-based approach to damage in soft fibered tissue, Biomechanics and modeling in mechanobiology 11 (2012) 595–608.

[49] L. Zhan, S. Wang, S. Qu, P. Steinmann, R. Xiao, A general continuum damage model for soft composites, Journal of the Mechanics and Physics of Solids 175 (2023) 105290.

[50] A. E. Ehret, M. Itskov, Modeling of anisotropic softening phenomena: application to soft biological tissues, International Journal of Plasticity 25 (5) (2009) 901–919.

[51] A. Hamedzadeh, T. C. Gasser, S. Federico, On the constitutive modelling of recruitment and damage of collagen fibres in soft biological tissues, European Journal of Mechanics-A/Solids 72 (2018) 483–496.

[52] A. Wehenkel, G. Louppe, Unconstrained monotonic neural networks, Advances in neural information processing systems 32 (2019).

[53] M. K. Rausch, G. P. Sugerman, S. Kakaletsis, B. Dortdivanlioglu, Hyper-viscoelastic damage modeling of whole blood clot under large deformation, Biomechanics and Modeling in Mechanobiology 20 (5) (2021) 1645–1657.

[54] E. Lorentz, S. Andrieux, A variational formulation for nonlocal damage models, International journal of plasticity 15 (2) (1999) 119–138.

[55] E. Lorentz, V. Godard, Gradient damage models: Toward full-scale computations, Computer Methods in Applied Mechanics and Engineering 200 (21-22) (2011) 1927–1944.

[56] D. Zuo, S. Avril, C. Ran, H. Yang, S. J. Mousavi, K. Hackl, Y. He, Sensitivity analysis of non-local damage in soft biological tissues, International Journal for Numerical Methods in Biomedical Engineering 37 (3) (2021) e3427.

[57] G. P. Sugerman, S. H. Parekh, M. K. Rausch, Nonlinear, dissipative phenomena in whole blood clot mechanics, Soft Matter 16 (43) (2020) 9908–9916.

[58] D. Balzani, S. Brinkhues, G. A. Holzapfel, Constitutive framework for the modeling of damage in collagenous soft tissues with application to arterial walls, Computer Methods in Applied Mechanics and Engineering 213 (2012) 139–151.

[59] C. Martin, W. Sun, Comparison of transcatheter aortic valve and surgical bioprosthetic valve durability: a fatigue simulation study, Journal of biomechanics 48 (12) (2015) 3026–3034.

Declaration of interests

☒ The authors declare that they have no known competing financial interests or personal relationships that could have appeared to influence the work reported in this paper.

☐ The authors declare the following financial interests/personal relationships which may be considered as potential competing interests: